JOURNAL OF CHEMICAL INFORMATION AND MODELING

Article

pubs.acs.org/jcim

Characterization of Heterocyclic Rings through Quantum Chemical Topology

Mark Z. Griffiths and Paul L. A. Popelier*

Manchester Institute of Biotechnology (MIB), 131 Princess Street, M1 7DN, Great Britain, and School of Chemistry, University of Manchester, Oxford Road, Manchester M13 9PL, Great Britain

Supporting Information

ABSTRACT: Five-membered rings are found in a myriad of molecules important in a wide range of areas such as catalysis, nutrition, and drug and agrochemical design. Systematic insight into their largely unexplored chemical space benefits from first principle calculations presented here. This study comprehensively investigates a grand total of 764 different rings, all geometry optimized at the B3LYP/6-311+G(2d,p) level, from the perspective of Quantum Chemical Topology (QCT). For the first time, a 3D space of local topological properties was introduced, in order to characterize rings compactly. This space is called RCP space, after the so-called ring critical point. This space is analogous to BCP space, named after the bond critical point, which compactly and successfully characterizes a chemical bond. The relative positions of the rings in RCP space are determined by the nature of the ring scaffold, such as the heteroatoms within the ring or the number of π-bonds. The summed atomic QCT charges of the five ring atoms revealed five features (number and type of heteroatom, number of π-bonds, substituent and substitution site) that dictate a ring's net charge. Each feature independently contributes toward a ring's net charge. Each substituent has its own distinct and systematic effect on the ring's net charge, irrespective of the ring scaffold. Therefore, this work proves the possibility of designing a ring with specific properties by fine-tuning it through manipulation of these five features.

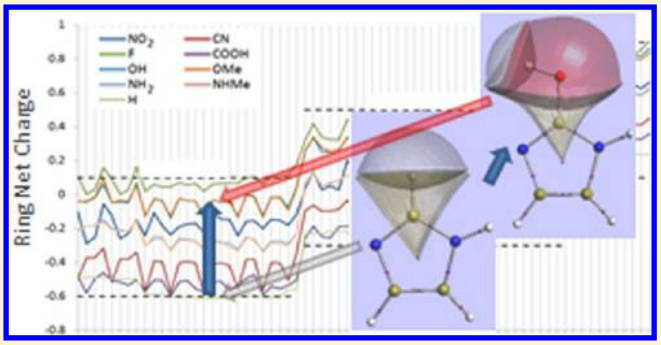

1. INTRODUCTION

The concept that chemical properties of a molecule determine its interactions with its environment is fundamental in many areas of chemistry. For example, the 3D and electronic structures of a molecule can determine if it binds to a protein and causes the desired effect. Altering the structure of the molecule results in a change to its properties and ultimately its interaction with the target. The desire to quantify the effects of alterations to molecules on their properties and how these changes to the properties cause changes in the molecule's behavior has led to an extensive literature.[1−9] The concept of chemical similarity is key to this work, where two molecules are said to be more similar in their behavior (such as interaction with the environment) as their properties become more similar. This comparison of molecules based on their similarity allows for relationships between molecules to be explored, such as finding alternative candidates for drug development. This is done by starting from a lead compound and selecting alternative molecules for development, where the candidates are chosen based on similarity to the lead. Many methods have been discovered for encoding the properties of a molecule for similarity comparisons.[10−13] The properties of the molecule tend to be stored in libraries or databases where an entry for each molecule or molecular fragment is assigned its calculated properties. This can lead to huge databases that may never truly cover all of chemical space due to the endless possibilities of variation within molecules. Cyclic molecules in particular require many data points to cover their region of chemical space as substitutions onto a ring can dramatically alter the rings' properties. Because of the large number of possible patterns of ring scaffold and substitution, much of the ring portion of chemical space has yet to be explored.[14,15] The five-membered ring systems targeted in this article contain rings that are found in a wide range of important molecules including antifungal drugs,[16] sedatives,[16] homogeneous catalysts,[17] multiple COX-2 inhibitors,[18−20] biosynthetic precursors,[21] and fungicides.[22]

Characterizations of rings and their properties tend to consider the ring as a whole, ignoring the individual atoms within the ring. This approach is due to the difficulty of expressing the properties of a single atom within the ring system, causing a ring to be treated as a single entity. The latter treatment does hold because the electron density within the ring is shared between the atoms of the ring. An obvious example is the electronic structure of the benzene ring, which has delocalized electrons within it. There are numerous studies that examine this delocalization of electron density throughout

Received: April 20, 2013
Published: June 24, 2013

dx.doi.org/10.1021/ci400235u | J. Chem. Inf. Model. 2013, 53, 1714−1725

the ring[23,24] and the measures of aromaticity calculated[25−29] to quantify these specific properties of a ring. Studies have also characterized the topological properties of rings.[30] Kolodzik et al. employed the molecular graphs of ring systems to characterize ring families.[31] These studies rarely consider the individual atoms of a ring. By characterizing the ring as a single system, the information regarding the atoms within the ring and their individual contributions to the ring properties can be lost. Therefore, this study aims to set up a method of characterizing rings not just as a whole but by the individual atoms within rings. This can be achieved through the use of Quantum Chemical Topology (QCT), which partitions a molecule into its constituent atoms, ultimately retrieving all information from a quantum mechanical wave function. QCT appears in many fields, including aromaticity,[32] QSAR/QSPR,[33,34] molecular dynamics simulations,[35] free radicals,[36] electron delocalization,[27] atom typing,[37] and hydrogen bonding.[38]

2. QUANTUM CHEMICAL TOPOLOGY

2.1. Gradient Vector Field and Critical Points. QCT partitions a molecule into its constituent atoms[39−41] based on the gradient vector field of the electron density, which is shown in Figure 1. How this works has been carefully explained in many places and will therefore not be repeated here. Figure 1 marks three of the four possible types of CP in 3D: triangles, circles, and squares. The different types of CP are categorized by the second derivatives of the electron density. Taking the second derivative of the electron density at a point results in three eigenvalues, λ_1, λ_2, and λ_3, which denote the curvature of the electron density in a local axis system.[40] A critical point can be categorized by the notation (ω, Z). Here, ω is the number of nonzero eigenvalues at this point, and Z is the sum of the signs of the eigenvalues, where +1 is allocated to a positive eigenvalue and −1 to a negative one. Therefore, a critical point at the nucleus (circle in Figure 1) has three eigenvalues that are all negative, which is summarized by the notation (3, −3). A bond critical point (BCP), shown as a square in Figure 1, is a saddle point in the electron density between two nuclei, denoted (3, −1), as it has two negative and one positive eigenvalue. A ring critical point (RCP; triangle) that lies within a cyclic system is written as (3, +1), given its two positive and one negative eigenvalue. There also exist cage critical points, or (3, +3), but they will not be discussed further.

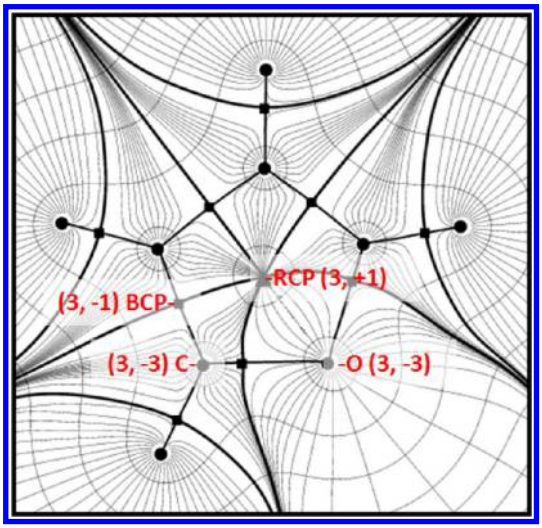

Figure 1. Superposition of constant electron density contour lines and the gradient vector field of the planar molecule furan. Interatomic surfaces are shown as bold curves bounding the topological atoms, while bonded nuclei are connected by bond paths (bold lines). Three types of critical points are shown: maximum at nucleus (or (3, −3); circle), bond critical point (BCP or (3, −1); square), and ring critical point (RCP or (3,+1); triangle).

The main focus of this work is on RCPs where the eigenvalues λ_2 and λ_3 are positive while λ_1 is negative and, by convention, $\lambda_3 > \lambda_2 > \lambda_1$. The two largest curvatures correspond to two mutually orthogonal directions in the so-called ring plane. In general, this ring plane is only planar in the vicinity of the RCP, but in the case of an aromatic ring, the ring plane is planar throughout the surface within the aromatic ring. The shape of the electron density at the RCP can be characterized by a convenient measure that compares the two local curvatures in the ring plane, λ_3 and λ_2, by simply taking their ratio. This leads to the ellipticity ε_{RCP}, which we define as $(\lambda_3/\lambda_2) - 1$. Because λ_3 is always larger than λ_2, the ellipticity ε_{RCP} is always positive but can, in theory, be zero when $\lambda_3 = \lambda_2$. This case corresponds to a perfectly cylindrical symmetry in the electron density at the RCP. In benzene, this situation is nearly reached, and ε_{RCP} amounts to about 2×10^{-4} at its RCP. Naturally, the shape of the electron density within the ring changes when ring atoms or substitutions to the ring vary. The electron density is pulled toward a given atom if its replacement is more electron withdrawing than the atom it replaced. Conversely, a replacement that is less electron withdrawing will resort in a greater congregation of the density at the RCP. Therefore, any changes in the atoms around the RCP will affect the electron density at the RCP, and the RCP properties will change accordingly.

2.2. Partitioning of the Electron Density. In order to generate single atom contributions toward a molecule's properties, the molecule is naturally partitioned through a pattern of gradient paths. This partitioning is illustrated for the planar heterocyclic aromatic furan in Figure 1. For example, a C and a H atom (e.g., top left) are separated in the plotting plane by two special gradient paths that terminate at a BCP. These two gradient paths are highlighted in bold and originate from infinity while both terminating at the leftmost BCP. Together, the two gradient paths actually represent the intersection between the plotting plane and the 3D Interatomic Surface (IAS) that separates the hydrogen atom from the carbon atom. An IAS that separates any two atoms inside the ring is slightly different in that now one of its gradient paths originates at a RCP instead of infinity. Overall, this topological partitioning defines the expected nine atoms in furan (Figure 1). The nuclei of the atoms act as attractors of gradient paths carving out the region allocated to a topological atom. This region is bound by the IASs surrounding these nuclei. The bond paths that intersect the IASs are gradient paths that begin at a BCP and terminate at a nucleus.

Figure 2 provides a 3D illustration of a topologically partitioned molecule, this time imidazole. Here, the gradient vector field is not explicitly shown, but the result of its action is: an aggregate of nine atoms, each allocated a subspace. This subspace is in principle infinite if we did not cap the whole molecule, and hence the atoms, by the 0.001 au isodensity surface, which usually serves as the practical boundary of an atom.

The atomic volume can be considered a "volume of influence" of the atom because the nucleus acts as an attractor

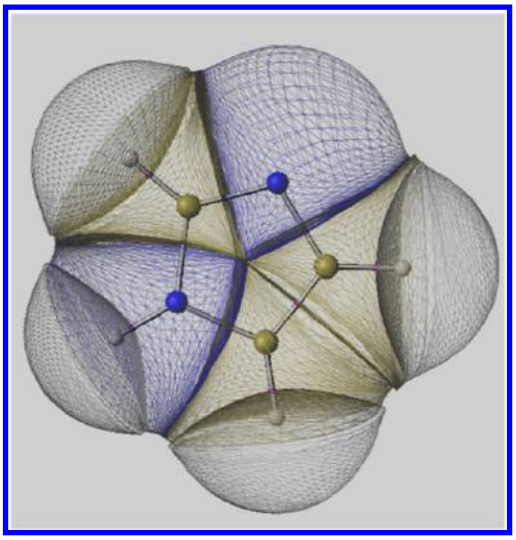

Figure 2. Imidazole topologically partitioned into finite-volume atoms capped by the 0.001 au isodensity envelope. Details of the drawing algorithm used are in ref 42.

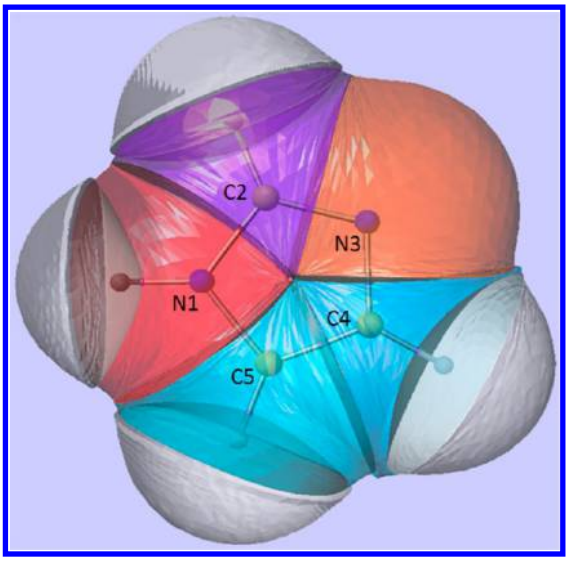

Figure 3. Relative net charges of non-hydrogen atoms within imidazole. The colors follow the rainbow spectrum where red is most negative and violet is most positive (see main text).

to the electron density within the atom. It can be obtained by integrating the unit function over the atomic volume. All atomic properties are obtained through one universal formula that expresses the volume integration of a given density over a topological atom's volume. For example, integrating the electron density yields the atomic population, which features strongly in this work. If this electronic population is supplemented with the nuclear charge, then one obtains the net (atomic) charge. If the integrand is a "local source" (which is a product of a Green's function and the Laplacian of the electron density), then chemical insight from the density of the RCP could be obtained, in terms of which ring atom contributes how much electron density to it. Such "source function"[43] study is part of future work, however.

Both Figures 1 and 2 clearly show that topological atoms do not overlap and that there are no gaps between them. Put together in their original position in the molecule, they exhaust 3D space and form the molecule. As a consequence of this perfect volumetric additivity, the concomitant atomic properties are also perfectly additive. A given property of a molecular fragment of interest, such as the ring atoms only or a methyl substituent, is therefore simply the sum of this property of each of the constituent atoms.

2.3. The Ring Critical Point and QCT Atoms. The QCT partitioning is able to reveal subtle changes in net charge. Figure 3 visualizes the changes in net charge observed in QCT atoms relative to their local environment. This figure shows the relative net charge for each non-hydrogen atom within imidazole with respect to the other atoms as a function of color on a scale that progress through the rainbow from red (most negative) to violet (most positive). The relative net charge for an atom is calculated by normalizing its net charge with the net charges of all five atoms of the ring. This calculation gives the atom's relative net charge as a value between 0 and 1 where 0 is the smallest and 1 is the largest value. The net charges for N1, C2, N3, C4, and C5 are −1.08, 0.82, −0.95, 0.32, and 0.28, respectively, with relative net charges 0, 1, 0.07, 0.74, and 0.71, respectively.

The carbon in between the two nitrogens (labeled C2 in Figure 3) is found to be much more positive relative to the other carbons within the ring, while the −NH nitrogen (N1) is more negative than the =N− nitrogen (N3). Interestingly, a difference in net charge also appears between the two adjacent carbons, although it is much more subtle. The carbon (C5) adjacent to the −NH nitrogen (N1, red) is actually slightly more negative than its neighboring carbon (C4) because the more negative nitrogen (N1) has a more pronounced effect on the carbon basin adjacent to it than the effect of the less negative nitrogen (N3 or =N−) on its adjacent carbon. These observations on QCT atoms show that an atom's element and local environment both affect the atom's properties. However, QCT atoms "perceive" changes not only within the ring structure but also due to substitutions, which are obviously lacking here.

Changes in substituents are reflected by changes in the ring atom the to which substituent is bonded. Figure 4 shows how the atomic basin of a carbon atom in imidazole changes when the hydrogen that is bonded to the carbon is substituted for an alcohol. The carbon basin is crushed upon substitution of the hydrogen with the alcohol. The oxygen of the alcohol has a much larger electronegativity than the hydrogen of the nonsubstituted imidazole. Therefore, a larger portion of the electron density between the carbon nucleus and the oxygen nucleus is attributed to the oxygen atom. The two nitrogen basins on either side of the carbon are also affected by the substitution. As the carbon basin is pushed downward, there is a noticeable splay in its basin at the CO IAS. At the outer ends of the IAS, the now wider carbon basin encroaches on both the nitrogen basins. Overall, substitution causes the boundaries of all atomic basins to be redrawn from the new electron density associated with the substitution.

As substituents are changed, the properties of the ring atoms adjust, and the interactions between the atoms within the ring also change. The RCP characterizes interactions between the ring atoms. If the RCP can accurately reflect the interactions between these ring atoms, then any changes in substituent would be visible in the RCP. This work aims at establishing whether the RCP can be used as a suitable representation of the atoms in the ring, and whether the RCP accounts for changes in atomic properties of ring atoms with respect to substitutions. Ultimately, this work attempts to characterize a ring in a

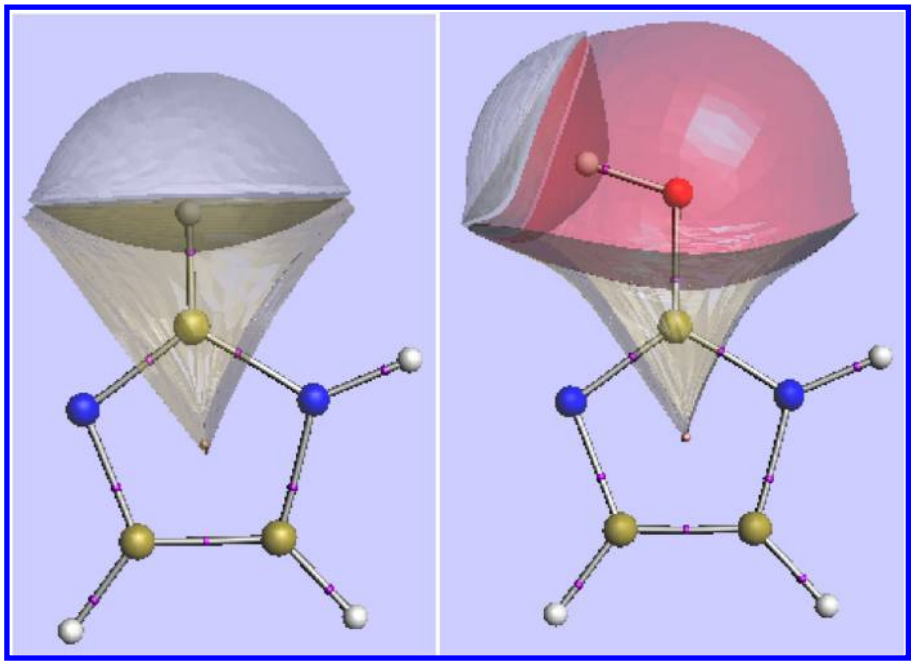

Figure 4. Imidazole (left) and imidazole-2-ol (right) focusing on changes in the shape of the atomic basin of the carbon directly affected by the substitution of H (left) with OH (right).

molecule using QCT properties calculated for the ring atoms only.

Only five-membered rings are considered in this article. However, the application of this work is not limited to the systems studied here because the QCT properties of an atom or a RCP are not directly affected by the number of atoms. It has been explained above that QCT properties are calculated for each topological atom individually. Therefore, the calculation of QCT properties for rings not studied here (e.g., six-membered rings or fused systems) requires summation over a different number of ring atoms. However, the behavior of a topological atom toward changes in the system it is part of follows the same principles discussed in this section (see Figures 3 and 4). Therefore, this work can easily be extended to different ring systems including fused ring systems, which only introduce a second RCP but are otherwise considered the same as any other ring with respect to its constituent atoms. For the sake of establishing the use of QCT for ring characterization, only simple five-membered ring systems are studied. This characterization begins with the RCP and is achieved through RCP space, which is explained just below.

3. METHODOLOGY

3.1. RCP Space. The concept of RCP space is inspired by that of BCP space,[44] which has been successfully used before.[45] If a BCP is accepted as a signature of a chemical bond, then it makes sense to evaluate properties at a BCP. The most straightforward property is the electron density itself, which can be related to bond order, provided the bonded atoms are the same. The same electron density value can appear at more than one BCP if one compares many different bonds *AB*, where *A* and *B* can be any element. However, if a second property is evaluated at a given BCP, then it becomes unlikely that two different BCPs share the same *two* property values. Typically, this second property is the Laplacian (of the electron density), which measures the local concentration of electron density and classifies bonds as closed-shell or shared interactions.[46] A third is the BCP ellipticity, which is not to be confused with the RCP ellipticity or ε_{RCP}. The former is defined as $(\lambda_2/\lambda_1) - 1$ and acts as a simple shape descriptor of electronic structure, for instance, expressing the π-character of a CC bond. If we imagine these three properties discussed above to span a 3D space, then each BCP appears as a point in this space. This was the original idea of BCP space,[44] which can of course be extended to an arbitrary number of dimensions. A molecule is then a cluster of points in BCP space, and this compact "quantum fingerprint" absorbs subtle changes due to substituent and conformational changes. Similarity between molecules can then be calculated in BCP space.[45,47,48]

RCP space is also spanned by the electron density, the Laplacian, and its own type of ellipticity ε_{RCP}. The RCP of a ring is plotted in RCP space using these three properties. RCP space assumes that the nature of the ring can be described by the electron density within the ring, that is, evaluated at the RCP in a similar fashion to BCP space, which assumes that a bond can be characterized by a single point in this space. The position of a ring in RCP space should show the nature of the ring and the nature of other rings with respect to it, based on their relative positions.

3.2. Calculation of RCP and Ring Atom Properties. To test the "RCP space hypothesis" discussed above, a large number of five-membered rings were geometry-optimized and their QCT properties then calculated. In order to firmly establish trends, it is important that a sizable number of rings are studied, the current set being the largest set investigated from a quantum chemical point of view, to the best of our knowledge. Figure 5 shows the general scaffold of the five-membered heteroatomic ring structures of the data set of molecules. This general scaffold consists of the ring scaffold (R*n*, n = 1−5) and the substituent scaffold (S*n*, n = 1−5). For each ring scaffold, only a single tautomer was considered because the rings are not connected to a molecule and are free to rotate in space. Therefore, different tautomers are identical if this rotation is allowed. For example, with the notation of

dx.doi.org/10.1021/ci400235u | J. Chem. Inf. Model. 2013, 53, 1714−1725

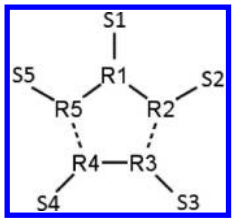

Figure 5. The general scaffold for the molecules of the data set. R*n* represents the ring atom where R = C, O, N, S, or P and *n* is the position on the ring. S*n* is a substitution on the ring and can be H, OH, OMe, NH_2, NHMe, NO_2^-, CN, F, COOH, or nothing if the adjacent ring atom is already at full valence, e.g. S, O, or =N−. The two dashed bonds can each be either a single or double bond.

Figure 5, the first tautomer of pyrazole has an NH at R1 and =N− at R3, a second tautomer has =N− at R1 and NH at R3. Relabeling the atoms of the second tautomer so that NH is once again at R1, then =N− becomes R3 and the second tautomer is now identical to the first. In this study, there are 30 different scaffolds of which 20 are unsaturated (see Figure 6b) and 10 saturated. The rings were varied in five fundamental aspects: (1) the number of heteroatoms in the ring (one to four), (2) the type of heteroatoms in the ring (nitrogen, oxygen, sulfur, and phosphorus), (3) the number of π-bonds within the ring (zero, one or two), (4) the substituent onto the ring (one of nine possibilities: H [nonsubstituted], OH, OMe, NH_2, NHMe, NO_2, CN, F, and COOH), and (5) the position of the substituent. The substituents were chosen to represent a range of simple substituents on rings. Only singly bonded substituents were considered to establish transferability of findings between rings because not all of the rings are able to form a double bond with a substituent, i.e. rings with two π-bonds lack the necessary sp^3 carbon. While most two-π-bond substituents are uncommon, the =O substituent found on many rings within large molecules is absent from this study. However, only a small portion of the rings in this study are able to form the necessary bond to the =O substituent.

Only monosubstituted structures were calculated. Considering the number of available substitution sites for the 20 unsaturated rings, there are 69 possible structures, each with eight possible substituents, totalling 572 = 8 × 69 + 20 ring structures, which includes the 20 nonsubstituted (or H substituted) rings. The set of unsaturated rings are shown in Table 1, where each ring has multiple entries denoting its

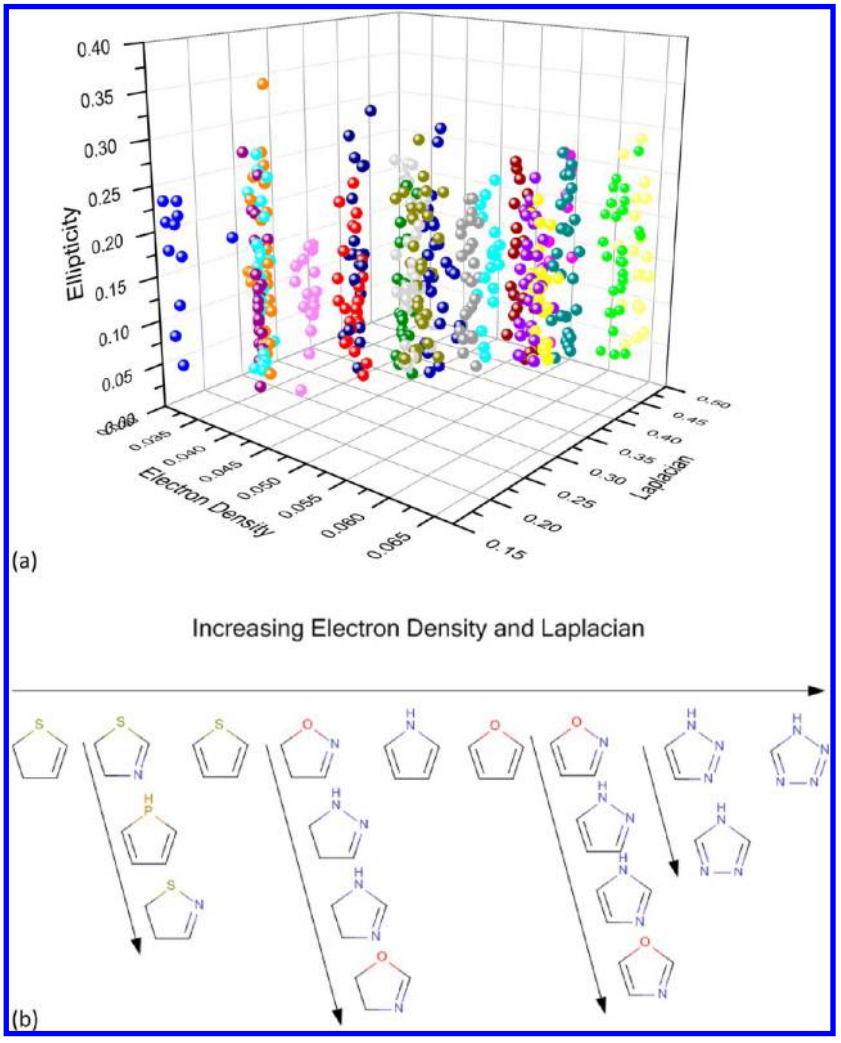

Figure 6. (a) RCP space for unsaturated (one or two π-bonds) five-membered heteroatomic rings. (b) Unsaturated five-membered heteroatomic rings in ascending order in RCP space. The descending arrows gather rings that overlap in RCP space. Following the arrows down corresponds to an increase of electron density and Laplacian at the RCP relative to the other rings. For example, imidazole rings tend to have a higher electron density and Laplacian at their RCP than pyrazole rings.

dx.doi.org/10.1021/ci400235u | *J. Chem. Inf. Model.* 2013, 53, 1714−1725

Table 1. Data Set of Unsaturated Ring Scaffolds Separated into the Different Substitution Sites Possible for Each Ring Scaffold

1	pyrazoline-1	24	1,2,4-triazole-3	47	isothiazoline-4
2	pyrazoline-3	25	1,2,4-triazole-5	48	isothiazoline-5
3	pyrazoline-4	26	tetrazole-1	49	thiazole-2
4	pyrazoline-5	27	tetrazole-5	50	thiazole-4
5	imidazoline-1	28	oxazoline-2	51	thiazole-5
6	imidazoline-2	29	oxazoline-4	52	isothiazole-3
7	imidazoline-4	30	oxazoline-5	53	isothiazole-4
8	imidazoline-5	31	isoxazoline-3	54	isothiazole-5
9	pyrrole-1	32	isoxazoline-4	55	thiophene-2
10	pyrrole-2	33	isoxazoline-5	56	thiophene-3
11	pyrrole-3	34	furan-2	57	1-thia-2,5-diazole-3
12	pyrazole-1	35	furan-3	58	1-thia-2,4-diazole-3
13	pyrazole-3	36	oxazole-2	59	1-thia-2,4-diazole-5
14	pyrazole-4	37	oxazole-4	60	phosphole-1
15	pyrazole-5	38	oxazole-5	61	phosphole-2
16	imidazole-1	39	isoxazole-3	62	phosphole-3
17	imidazole-2	40	isoxazole-4	63	phosphazole-2
18	imidazole-4	41	isoxazole-5	64	phosphazole-4
19	imidazole-5	42	furazan-3	65	phosphazole-5
20	1,2,3-triazole-1	43	thiazoline-2	66	isophosphazole-3
21	1,2,3-triazole-4	44	thiazoline-4	67	isophosphazole-4
22	1,2,3-triazole-5	45	thiazoline-5	68	isophosphazole-5
23	1,2,4-triazole-1	46	isothiazoline-3	69	1-phospho-2,5-diazole-3

available substitution sites. This study contains 572 unsaturated rings and 192 saturated rings, leading to a grand total of 764 different rings. The molecules were optimized with GAUSSIAN 03[49] at the B3LYP/6-311+G(2d,p) level of theory. The QCT atomic properties and the three local properties (evaluated at the RCP) were calculated for all geometry-optimized molecules using MORPHY01.[50] Each molecule was positioned in RCP space according to their electron density, Laplacian, and ellipticity at the RCP.

4. RESULTS AND DISCUSSION

4.1. Rings in RCP Space. Figure 6a shows the RCP space for the unsaturated rings. Only the unsaturated rings are shown to maintain clarity. Only showing the unsaturated rings is sufficient because trends in RCP space positions found within the two π-bond ring (scaffolds) are the same for the one π-bond and no π-bond rings. Similarly, trends between the two π-bond and one π-bond ring sets are repeated between the one π-bond and no π-bond ring sets. In Figure 6a, each color corresponds to structures with a common ring scaffold where the number of points for each scaffold is determined by all of the possible monosubstituted structures as outlined in Figure 5. For example, each of the red points represents a mono-substituted 1,2,3-triazole ring where substitution type and position are varied. By coloring the data points in such a way, it becomes clear that all points for a defined ring scaffold occupy the same region of RCP space. Therefore, RCP space can distinguish between ring types. The way the rings appear in RCP space highlights trends in the relative positions of the ring scaffolds. These trends are found by examining each separate ring scaffold (separate colors in Figure 6a). Figure 6b shows these trends when examined from the lowest values in both the electron density and Laplacian, to the highest electron density and Laplacian, i.e. moving in a sequence from left to right in Figure 6a. Rings that overlap in RCP space are shown as branches in Figure 6b, where following the arrows down corresponds to an increase of electron density and Laplacian at the RCP relative to the other rings. For example, pyrazole rings are higher up in RCP space than pyrrole rings, and imidazole rings are higher up in space than pyrazole but with an overlap between the pyrazole and imidazole ring sets. Figure 6b shows that there are three variables in the ring scaffold that affect its position in RCP space: (i) the number of π-bonds, (ii) which element a given heteroatom is, and (iii) the number of heteroatoms.

First the trends within two π-bond rings are examined (which are the same for the one and no π-bond rings), followed by the trends between two and one π-bond rings. The lowest two π-bond rings correspond to rings with a single phosphorus or sulfur atom within the ring. Moving on to the next set of rings in the aforementioned sequence, rings are found containing a single nitrogen or oxygen atom within the ring. These rings are followed by rings containing a second heteroatom within the ring. These are followed by rings with a third heteroatom and finally a fourth heteroatom within the ring. Therefore, as the element of the heteroatom changes from phosphorus or sulfur to nitrogen or oxygen, the ring's position in RCP space from left to right. Similarly, an increase in the number of heteroatoms within the ring moves the ring's position from left to right in RCP space. These trends are repeated for the rings with a single π-bond. For example, the leftmost ring (in Figure 6b) contains one sulfur. When another heteroatom is added to the ring (column two of Figure 6b), it moves to the right in RCP space (Figure 6a). If the sulfur in the two-heteroatom ring is replaced by a nitrogen or oxygen (column four of Figure 6b), the ring moves further to the right in RCP space. However, there is an overlap between the three sets (zero, one, or two π-bonds), where rings most left in RCP space of a π-bond set overlap with the rings highest in the RCP space for the previous π-bond set. An example of this is that of the overlap between rings containing a single sulfur with two π-bonds (column three of Figure 6b) and rings with two heteroatoms and a single π-bond (column four of Figure 6b). This overlap suggests that the increased number of heteroatoms

dx.doi.org/10.1021/ci400235u | J. Chem. Inf. Model. 2013, 53, 1714−1725

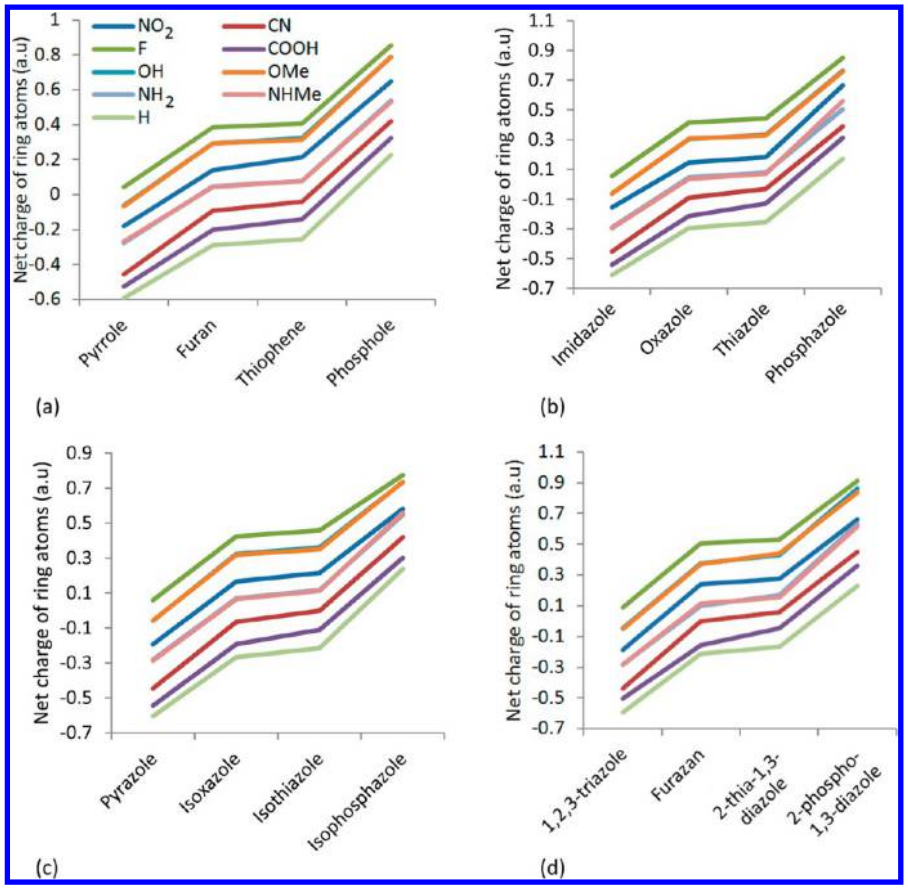

Figure 7. Net charges for ring atoms of substituted five-membered heterocycles where the heteroatom at the first position (R1 in Figure 5) is changed from nitrogen to oxygen, to sulfur, and then to phosphorus for (a) single heteroatom ring scaffolds, (b) a nitrogen added to the scaffolds at R3, (c) a nitrogen added to the scaffolds at R2, and (d) a nitrogen added to the scaffolds at R2 and R3.

in the rings with a single π-bond creates an electron density at the RCP comparable to that of rings with two π-bonds but containing fewer heteroatoms donating electron density to the ring. Because the rings in RCP space form this progression, the ring scaffold of an unknown ring can be determined through its position in RCP space relative to other rings. Rings can be categorized using only the electron density, Laplacian, and ellipticity at the RCP.

In an attempt to quantify differences in the ring types in RCP space, the effects of ring alterations and distances in RCP space were examined. Consistent changes in RCP properties can predict similar changes for unknown ring scaffolds. It is possible to move through RCP space by making calculated alterations to a ring to alter its properties to match the desired properties. For example, a nitrogen atom was inserted into a furan ring replacing the carbon at the second or third position, forming isoxazole and oxazole, respectively. The difference in electron density at the RCP between isoxazole and furan, and oxazole and furan, were calculated for all nine ring substituents attached to the ring. The mean change in electron density from furan to isoxazole was −0.015 au. The largest change was −0.020 au and the smallest −0.012 au, or an interval of only 0.008 au. On the other hand, the mean change in electron density on going from furan to oxazole was −0.058 au. Here, the change in electron density ranged from −0.052 to −0.064 au, again an interval of 0.008 au. The substituted derivatives of isoxazole and of oxazole display consistent changes in electron density at the RCP when a nitrogen is substituted into the ring. The difference in the position of the added nitrogen is also visible in the RCP position as both isoxazole and oxazole have no overlap in their ranges, and the difference between the mean changes for both is much larger than the ranges for either. RCP properties have been found to distinguish between ring scaffolds, and RCP space can be navigated where changes in RCP properties are relevant to a ring's position in RCP space.

4.2. Effect of Heteroatom on Ring Properties. It has been established that RCP space can distinguish between ring scaffolds. However, RCP space alone cannot clearly discern between substitutions onto a ring with respect to type and position of substitution. Therefore, to account for substitutions onto a ring, the properties of the QCT atoms of the ring (R1 to R5 in Figure 5) are introduced because QCT atomic basins are significantly changed when the local environment is altered (see Figure 4). Therefore, properties of the QCT atoms within the ring can reflect any changes in the substituents on the ring.

The effects of substituents and ring scaffold on the properties of the QCT atoms are determined with the same data set of rings as in the RCP space. The ring properties were calculated using only the five atoms in the ring, while the hydrogens and atoms of the substituents were not included. Therefore, the ring atom properties will indicate how the five atoms in the ring change due to ring scaffold and substitution changes.

Figure 7a shows the net charges for the ring atoms of four different rings, each with nine different substitutions. The four ring scaffolds differ by the element of the heteroatom in the ring in the order nitrogen, oxygen, sulfur, and phosphorus along the x axis from left to right. The net charges for each substitution run parallel to the other substitutions across all

dx.doi.org/10.1021/ci400235u | J. Chem. Inf. Model. 2013, 53, 1714−1725

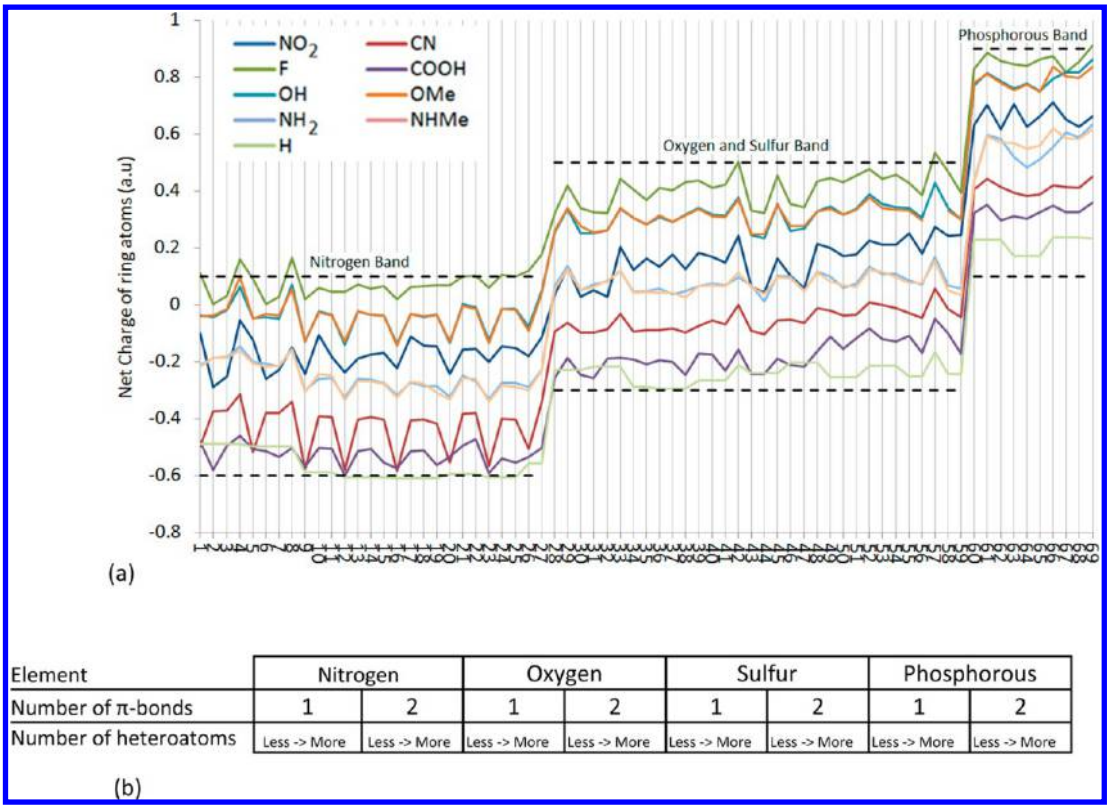

Figure 8. (a) Net charge of ring atoms for five membered heterocyclics with respect to ring scaffolds and substituents. The numbers along the *x* axis correspond to the rings of Table 1 (all values are given in Table S1 of the Supporting Information). (b) Hierarchy of ordering scheme used for panel (*a*).

four ring scaffolds. The parallel nature of the net charges suggests that each substituent has a defined, and consistent, effect on the net charge of the atoms in the ring. Figure 7b–d show that this observation holds for other rings as well. The difference between the ring scaffolds between panels a–d is the number and position of the heteroatoms in the ring. The atom in the first position in the ring is the only difference between the ring scaffolds along the *x* axis of each panel. For example, in Figure 7b, all ring scaffolds have a nitrogen at the third position of the ring (R3), while the heteroatom that changes between scaffolds is at the first position. Figure 7c has a similar scaffold to Figure 7b, but the nitrogen is at the second position of the ring (R2). Figure 7d has scaffolds with two nitrogens (at R2 and R5) and a third heteroatom (at R1) that varies across the *x* axis. Close observation of all four panels reveals that the pair of substitutions OH and OMe are almost perfectly superimposed, which is also true for the NH_2 and NHMe substitution pair. This suggests that the addition of the methyl group to the substituent has little effect on how the substitution is "seen" by the atoms within the ring.

4.3. Effect of Ring Scaffold on Ring Properties. These trends and observations of the parallel lines are consistent throughout all four of the panels. Figure 8a extends the analysis to the entire data set, and the observations and trends of Figure 7 are still present. It is worth noting that there are cases where the parallel nature of the substitution lines is broken and lines cross where they are not expected to. These unexpected net charges occur when a nitro is substituted onto an sp^3 carbon, producing net charges similar to or lower than NH_2 and NHMe where the net charge for the nitro is expected to be larger.

Figure 8a shows all the nonsaturated ring molecules with substitutions, and the hierarchy of how the rings scaffolds were ordered in Figure 8a is shown in Figure 8b. The schematic in Figure 8b shows the priorities, by row, of how the rings were ordered. First, the rings were separated (from left to right as in Figure 7a–d) into nitrogen, oxygen, sulfur, and phosphorus containing ring scaffolds where nitrogen was the only heteroatom present in the nitrogen rings (e.g., pyrrole and imidazole), but some of the other rings contain nitrogens as well as their element (e.g., furan, oxazole for oxygen and thiophene, thiazole for sulfur). The ring scaffolds within each of these groupings are prioritized by the number of π-bonds within the ring, shown by the second row of Figure 8b. The first half of the grouping consists of single π-bond ring scaffolds, while the second half consists of ring scaffolds with two π-bonds. Finally, the ring scaffolds within each of the π-bond groupings (single or double) are ordered by an increasing number of heteroatoms within the ring scaffold, going from left to right, as shown in row three of Figure 8b. All the rings in Figure 8a have been placed in a systematic order where ring scaffolds are grouped based on the characteristics shown in Figure 8b.

The systematic ordering of all rings in three rows (see Figure 8b) reveals the relationships between ring scaffolds and the relative effects of structural variations within ring scaffolds. The first division of the data set is into the elements (N, O, S, and P) of the heteroatoms within the ring (row 1 in Figure 8b). Splitting and ordering the rings into their main elements (similar to Figure 7a–d) recreates the shape of these graphs in Figure 8a but now for the extended data set. In all graphs of Figure 7a–d, the nitrogen rings have the lowest net charge,

Table 2. Change in Net Charge upon Substitution onto a Nonsubstituted Ring for Eight Functional Groups Split into the Three Possible Atom Types for the Site of the Substitution

		NO_2	CN	F	COOH	OH	OMe	NH_2	NHMe
	mean	0.29	0.14	0.55	−0.01	0.48	0.50	0.30	0.29
sp^2 C	standard deviation	0.07	0.02	0.05	0.04	0.03	0.04	0.03	0.02
	S. D. %	25	18	8	510	7	8	10	8
	mean	0.42	0.20	0.66	0.08	0.56	0.56	0.33	0.32
sp^3 C	standard deviation	0.07	0.04	0.07	0.06	0.06	0.07	0.03	0.03
	S. D. %	16	20	10	75	11	12	8	8
	mean	0.38	0.03	0.64	0.02	0.47	0.47	0.28	0.27
N	standard deviation	0.02	0.02	0.03	0.02	0.01	0.01	0.01	0.01
	S. D. %	6	74	5	83	2	2	3	4

*Values in table only shown to 2 d.p.

followed by oxygen and sulfur, which are relatively similar, and finally the phosphorus rings. This shape is recreated by the extended data set where rings grouped by the same element form three distinct bands. The lowest band, which is between a net charge of −0.6 and 0.1, consists of nitrogen ring scaffolds, followed by the oxygen and sulfur scaffolds where both form a single band that lies between a net charge of −0.3 and 0.5, and finally the phosphorus band between a net charge of 0.1 and 0.9.

The second level in dividing the data set regards a partition within each of the element groupings; the rings are separated by the number of π-bonds within the ring, where the number of π-bonds increases from one to two going from left to right (row 2 in Figure 8b). For all three large groups, nitrogen, oxygen, and sulfur, the ring patterns with fewer π-bonds tend to be more erratic in net charge than ring patterns with more π-bonds. This shows that the net charge is affected differently upon substitution when the substitution site is an sp^3 atom compared to an sp^2 atom. This difference in the net charge is noticeable and causes erratic spikes in the net charge. The erratic spikes are not seen in systems with two π-bonds because every atom has sp^2 hybridization, except when atom R1 (Figure 5) is a nitrogen with a hydrogen at S1, but this case is discussed later. The ring scaffolds with sp^3 atoms still contain one π-bond and are therefore a mixture of sp^3 and sp^2 atoms. In summary, the atom type (sp^3 carbon, sp^2 carbon or N(−H)) where substitution occurs affects the ring properties.

The third and final division used to order the rings concerns the number of heteroatoms within the ring scaffold. For a π-bond grouping, all of the ring scaffolds within the grouping were ordered from the smallest to the largest number of heteroatoms within the ring (row 3 in Figure 8b). For example, for the grouping of nitrogen with two π-bonds, the four ring scaffolds are ordered pyrrole (one nitrogen), pyrazole (two nitrogens), triazole (three nitrogens), and tetrazole (four nitrogens). Increasing the number of heteroatoms within the ring tends to increase the net charge of the ring. This is most evident when examining the groupings with two π-bonds in Figure 8a, because the difference in net charge between substitutions at an sp^2 or sp^3 atom (discussed above) is greater than the difference in net charge between rings of an increasing number of heteroatoms. Therefore, any changes in net charge due to an increase in number of heteroatoms are masked by the change in net charge upon substitution onto atoms of differing hybridization. Figure 8a expresses this masking by spikes in its largely parallel profiles, which occur in three regions, one of which ranges from ring 28 to 33. Rings with two π-bonds do not suffer from this masking because all atoms have the same hybridization. This, in turn, is expressed by flatter profiles, which occur between rings 34 and 41 (Figure 8a), for example.

By ordering the rings in the manner described above (Figure 8b), a *ring scaffold hierarchy* is created with three levels to the hierarchy (rows of Figure 8b). Each of the levels of the hierarchy has a specific effect on the net charge. This effect is independent of grouping at any of the three levels. In other words, changes in net charge due to the number of heteroatoms in the ring scaffold (row 3, Figure 8b) are consistent irrespective of whether the ring is in the nitrogen, oxygen, sulfur, or phosphorus groupings (row 2), or in groupings with single or double π-bonds (row 2).

Substituents (Sn in Figure 5) also affect the net charge, independently of variation within the ring scaffold (3 rows in Figure 8b), because the substituents form parallel lines in Figure 8a. The effect of the substituent can also be incorporated into this hierarchy where changes within a ring (R*n*, Figure 5) or to its substitutions (S*n*, Figure 5) affect the net charge of the ring systematically with respect to these changes. Therefore, manipulation of the ring scaffold structure or substituent allows for selectively creating a ring of a desired net charge, if the substitutions on the rings remain constant. For example, if a mono-fluoro-substituted ring were needed with a net charge of 0.05 au, then pyrazole is the ring of choice, as can be deduced from Figure 8a. If a need arose to fine-tune this net charge by decreasing it slightly, then one should replace a ring nitrogen with a ring carbon (forming pyrrole), decreasing the net charge by 0.03 au. Conversely, the addition of a nitrogen to the ring (forming triazole) increases the net charge by 0.1 au

4.4. Effect of Substitution on Ring Properties. Now we are in a position to exploit the parallel nature of the profiles of net charge variation throughout the set of ring scaffolds in Table 1. More precisely, one can move from one profile to another and observe a change in net charge specific to a change in substituent. This observed change in substitution and net charge can be applied for prediction purposes. For example, the change in net charge going from a nonsubstituted to an F substituted ring is approximately 0.6 au for all rings. Predictions can be made by taking the nonsubstituted ring and adding the mean change in net charge for each substitution. Therefore, if the net charge of a ring scaffold (Rn in Figure 5) is known, then the new net charge of the substituted ring can be predicted. This procedure can be repeated for many cases in an attempt to recover the shape of Figure 8a using only these predicted values. The result is shown in Figure S1 of the Supporting Information. While the general shape of Figure 8a can be recovered, there are many local peaks that are absent from the predicted profiles. The local peaks are due to the different sites

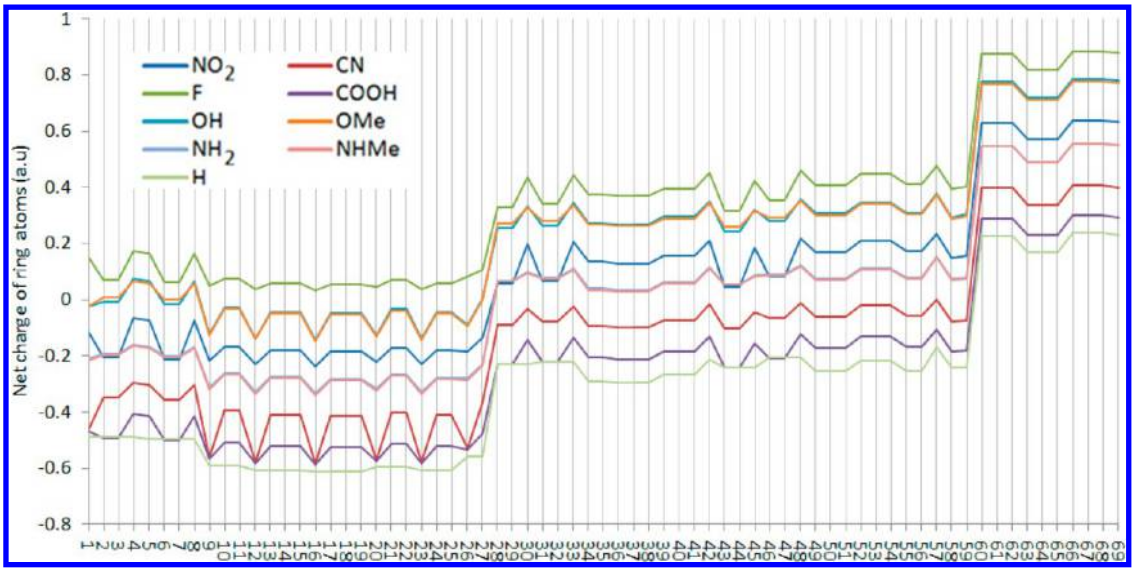

Figure 9. Ring atom net charges predicted from the sum of a mean net charge change of a given substitution onto different atom types (sp^3 carbon, sp^2 carbon, or N(−H)) and the net charge of a nonsubstituted ring.

of substitution, which are not considered in the calculation of the mean change.

In order to recover the peaks that are absent, one must account for the site of the substitution in the calculation of the mean change in net charge. This calculation was refined by calculating a separate mean for substitutions onto nitrogens (N−H) or sp^2 or sp^3 carbons. Table 2 shows the mean net charge change for each substitution with respect to the site of the substitution, as well as the corresponding standard deviations, and the latters' proportion (as %) of the respective means. For each of the substituted rings, the appropriate mean change in net charge (determined in Table 2) was applied to the nonsubstituted ring's net charge. In all cases except five, the standard deviation of the change in net charge is below 20% of the mean change in net charge. Therefore, the changes in net charge due to substitution are similar within each substituent and site. COOH substitutions have a very large standard deviation relative to mean change. However, this may be due to the small mean change (i.e., −0.01) between COOH and nonsubstituted rings. The high percentage is caused by a typical standard deviation being divided by an atypically small mean. Indeed, the COOH substitution (0.04, 0.06, and 0.02, for sp^2 C, sp^3 C, and N, respectively) is similar to the standard deviations of all other substituents (ranging from 0.02 to 0.07, 0.03 to 0.07, and 0.01 to 0.03, for sp^2 C, sp^3 C, and N, respectively), but the mean change is much smaller. Figure 9 shows the prediction of ring net charge where the appropriate mean change for each substitution with respect to the site of the substitution is applied. Comparing the new predictive model (Figure 9) to the original calculated values (Figure 8a) shows that the majority of peaks are now present in the graph where they were absent when the substitution site was ignored.

Finally, it should be mentioned that the way substituents alter the electronic charge of the ring can be linked to physicochemical properties such as the Hammett constants. Work from this group published elsewhere[51] shows that the ring net charges for the substituents in both furan and imidazole match the order of the Hammett constants, when only the π electrons were considered.

5. CONCLUSION

This study characterizes both rings and the atoms within rings using quantum chemical topology. It provides a wealth of data for 764 ring structures, some of which have found potential use in antifungal drugs, sedatives, homogeneous catalysts, COX-2 inhibitors, biosynthetic precursors, and fungicides. The study was targeted at five-membered heterocyclic rings varying in the number of heteroatoms, type of heteroatoms, position of heteroatoms in the ring, number of π-bonds, substituent, and position. All rings were monosubstituted only.

An entire ring system, with substitutions, was characterized through three properties calculated at the ring critical point: the electron density, its Laplacian, and a new type of ellipticity, which together form a 3D space called RCP space. Rings with an increasing structural commonality have a decreasing distance in RCP space. The positions of the rings in RCP space are determined by the ring scaffolds. Therefore, chemically meaningful sequences of rings emerged in this RCP space.

To determine the effects of the individual ring atoms on the ring's properties, the composition of the rings was compared to the ring's properties. Five features of a ring and its substitutions were found where each feature was independently responsible for the ring's properties. These were (i) the elements of the atoms within the ring, (ii) the number of heteroatoms, (iii) the number of π-bonds, (iv) the substituent, and (v) the ring atom to which the substituent was bonded. By varying each of these features, changes to a ring's properties can be controlled. If the substituent and its position on the ring are altered, then the change in ring property upon alteration can be predicted. By using both ring properties and ring atom properties, rings can be successfully characterized where any differences in the ring's scaffold or substitution are reflected in the calculated properties. For the average change in net charge of the ring atoms upon substitution 5 out of 24 standard deviations were below 20% of the average change. Therefore, each substituent has its own distinct and *systematic* effect on the ring's net charge, *irrespective of the ring scaffold*. In other words, the present study reveals an "orthogonality" between substituent and ring. Therefore, the change in net charge for each of the substitutions onto any ring atom can be predicted because the substituents each cause their

own signature change to the net charge. The RCP properties and ring atom properties do not explicitly involve the number of atoms in the ring (set at five here). Therefore, we expect that this method can be extended to ring systems of any size, including fused ring systems.

■ ASSOCIATED CONTENT

Supporting Information

Table S1. Ring net charges for all unsaturated rings studied (572 rings), separated into substitution sites and substituents. The rings correspond to the 69 scaffolds of Table 1 and all listed values are plotted in Figure 8a. **Figure S1.** Ring atom net charges predicted from the sum of a mean net charge change of a given substitution and the net charge of a nonsubstituted ring. This material is available free of charge via the Internet at http://pubs.acs.org.

■ AUTHOR INFORMATION

Corresponding Author

*E-mail: pla@manchester.ac.uk.

Notes

The authors declare no competing financial interest.

■ REFERENCES

(1) Lameijer, E. W.; Kok, J. N.; Back, T.; Ijzerman, A. P. Mining a chemical database for fragment co-occurrence: Discovery of "chemical cliches". *J. Chem. Inf. Model.* **2006**, *46*, 553−562.

(2) Ertl, P. Cheminformatics Analysis of Organic Substituents: Identification of the Most Common Substituents, Calculation of Substituent Properties, and Automatic Identification of Drug-like Bioisosteric Groups. *J. Chem. Inf. Comput. Sci.* **2003**, *43*, 374−380.

(3) Holliday, J. D.; Jelfs, S. P.; Willett, P.; Gedeck, P. Calculation of Intersubstituent Similarity Using R-Group Descriptors. *J. Chem. Inf. Comput. Sci.* **2003**, *43*, 406−411.

(4) Lima, L. M. A.; Barreiro, E. J. Bioisosterism: A useful strategy for molecular modification and drug design. *Curr. Med. Chem.* **2005**, *12*, 23−49.

(5) Patani, G. A.; LaVoie, E. J. Bioisosterism: A rational approach in drug design. *Chem. Rev.* **1996**, *96*, 3147−3176.

(6) Wermuth, C.-G. Molecular variations based on bioisosteric replacements. In *The Practice of Medicinal Chemistry*; Wermuth, C.-G., Ed.; Academic Press: London, 1996; pp 202−237.

(7) Olesen, P. H. The use of bioisosteric groups in drug design. *Curr. Opin. Drug Discovery Dev.* **2001**, *4*, 471−478.

(8) Devereux, M.; Popelier, P. L. A.; McLay, I. M. The Quantum Isostere Database: a web-based tool using Quantum Chemical Topology to predict bioisosteric replacements for drug design. *J. Chem. Inf. Model.* **2009**, *49*, 1497−1513.

(9) Graham, J. E.; Ripley, D. C.; Smith, J. T.; Smith, V. H. J.; Weaver, D. F. Theoretical studies applied to drug design: ab initio electronic distributions in bioisosteres. *J. Mol. Struct.: THEOCHEM* **1995**, *343*, 105−109.

(10) Sheridan, R. P. The most common chemical replacements in drug-like compounds. *J. Chem. Inf. Comput. Sci.* **2002**, *42*, 103−108.

(11) Kier, L. B.: *Molecular Structure Description: The Electrotopological State*; Academic: San Diego, CA, 1999.

(12) Cruciani, C.; Crivori, P.; Carrupt, P. A.; Testa, B. Molecular fields in quantitative structure-permeation relationships: the VolSurf approach. *J. Mol. Struct.: THEOCHEM* **2000**, *503*, 17.

(13) Jennings, A.; Tennant, M. Selection of Molecules Based on Shape and Electrostatic Similarity: Proof of Concept of "Electroforms. *J. Chem. Inf. Model.* **2007**, *47*, 1829−1838.

(14) Ertl, P.; Jelfs, S.; Muhlbacher, J.; Schuffenhauer, A.; Selzer, P. J. Quest for the rings - in silico exploration of ring universe to identify novel bioactive heteroaromatic scaffolds. *J. Med. Chem.* **2006**, *49*, 4568.

(15) Pitt, W. R.; Parry, D. M.; Perry, B. G.; Groom, C. R. Heteroaromatic rings of the future. *J. Med. Chem.* **2009**, *52*, 2952−2963.

(16) Katritzky, A.; Rees, C. *Comprehensive Heterocyclic Chemistry*; Pergamon Press: Oxford, Great Britain, 1984; Vol. *5*.

(17) Liu, H.; Du, D. M. Recent Advances in the Synthesis of 2-Imidazolines and Their Applications in Homogeneous Catalysis. *Adv. Synth. Catal.* **2009**, *351*, 489−519.

(18) Talley, J. J.; Brown, D. L.; Carter, J. S.; Graneto, M. J.; Koboldt, C. M.; Masferrer, J. L.; Perkins, W. E.; Rogers, R. S.; Shaffer, A. F.; Zhang, Y. Y. 4-[5-Methyl-3-phenylisoxazol-4-yl]-benzenesulfonamide, valdecoxib: a potent and selective inhibitor of COX-2. *J. Med. Chem.* **2000**, *43*, 775.

(19) Steinbach, G.; Lynch, P. M.; Phillips, R. K.; Wallace, M. H.; Hawk, E.; Gordon, G. B.; Wakabayashi, N.; Saunders, B.; Shen, Y.; Fujimura, T. The effect of celecoxib, a cyclooxygenase-2 inhibitor, in familial adenomatous polyposis. *N. Engl. J. Med.* **2000**, *342*, 1946−1952.

(20) Yang, C. Y.; Meng, C. L.; Liao, C. L.; Wong, P. Y. K. Regulation of cell growth by selective COX-2 inhibitors in oral carcinoma cell lines. *Prostaglandins Other Lipid Mediators* **2003**, *72*, 115−130.

(21) Lehninger, A.; Nelson, D. L.; Cox, M. M. *Lehninger Principles of Biochemistry*, 5th ed.; W. H. Freeman: New York, 2008.

(22) Gisi, U.; Sierotzki, H.; Cook, A.; McCaffery, A. Mechanisms influencing the evolution of resistance to Qo inhibitor fungicides. *Pest Manage. Sci.* **2002**, *58*, 859−867.

(23) Poater, J.; Duran, M.; Sola, M. Analysis of electronic delocalization in buckminsterfullerene (C-60). *Int. J. Quantum Chem.* **2004**, *98*, 361−366.

(24) Matta, C. F.; Hernandez-Trujillo, J. Bonding in polycyclic aromatic hydrocarbons in terms of the electron density and of electron delocalization. *J. Phys. Chem. A* **2003**, *107*, 7496−7504.

(25) Krygowski, T. M.; Ejsmont, K.; Stepien, B. T.; Cyranski, M. K.; Poater, J.; Sola, M. Relation between the substituent effect and aromaticity. *J. Org. Chem.* **2004**, *69*, 6634−6640.

(26) Poater, J.; Sola, M.; Viglione, R. G.; Zanasi, R. Local aromaticity of the six-membered rings in pyracylene. A difficult case for the NICS indicator of aromaticity. *J. Org. Chem.* **2004**, *69*, 7537−7542.

(27) Poater, J.; Fradera, X.; Duran, M.; Sola, M. The delocalization index as an electronic aromaticity criterion: Application to a series of planar polycyclic aromatic hydrocarbons. *Chem.—Eur. J.* **2003**, *9*, 400−406.

(28) Sjoberg, P.; Murray, J. S.; Brinck, T.; Politzer, P. Average Local Ionization Energies on the Molecular-Surfaces of Aromatic Systems as Guides to Chemical-Reactivity. *Can. J. Chem.* **1990**, *68*, 1440−1443.

(29) Murray, J. S.; Abu-Awwad, F.; Politzer, P. Characterization of aromatic hydrocarbons by means of average local ionization energies on their molecular surfaces. *J. Mol. Struct.: THEOCHEM* **2000**, *501*, 241−250.

(30) Berger, F.; Flamm, C.; Gleiss, P. M.; Leydold, J.; Stadler, P. F. Counterexamples in Chemical Ring Perception. *J. Chem. Inf. Comput. Sci.* **2004**, *44*, 323−331.

(31) Kolodzik, A.; Urbaczek, S.; Rarey, M. Unique Ring Families: A Chemically Meaningful Description of Molecular Ring Topologies. *J. Chem. Inf. Model.* **2012**, *52*, 2013−2021.

(32) Bultinck, P.; Rafat, M.; Ponec, R.; Van Gheluwe, B.; Carbó-Dorca, R.; Popelier, P. L. A. Electron delocalization and aromaticity in linear polyacenes: atoms in molecules multicenter delocalization index. *J. Phys. Chem. A* **2006**, *110*, 7642−7648.

(33) Popelier, P. L. A.; Chaudry, U. A.; Smith, P. J. Quantum topological molecular similarity. Part 5. Further development with an application to the toxicity of polychlorinated dibenzo-p-dioxins (PCDDs). *J. Chem. Soc., Perkin Trans. 2* **2002**, 1231−1237.

(34) O'Brien, S. E.; Popelier, P. L. A. Quantum Topological Molecular Similarity. Part 4: A QSAR study of Cell Growth Inhibitory Properties of Substituted (E)-1-Phenylbut-1-en-3-ones. *J. Chem. Soc., Perkin Trans. 2* **2002**, 478−483.

(35) Liem, S. Y.; Popelier, P. L. A.; Leslie, M. Simulation of liquid water using a high rank quantum topological electrostatic potential. *Int. J. Quantum Chem.* **2004**, *99*, 685−694.
(36) Singh, N. K.; Popelier, P. L. A.; O'Malley, P. J. Substituent effects on the stability of para-substituted benzyl radicals. *Chem. Phys. Lett.* **2006**, *426*, 219−221.
(37) Aicken, F. M.; Popelier, P. L. A. Atomic properties of selected biomolecules. Part 1. The interpretation of atomic integration errors. *Can. J. Chem.* **2000**, *78*, 415−426.
(38) Joubert, L.; Popelier, P. L. A. The prediction of energies and geometries of hydrogen bonded DNA base-pairs via a topological electrostatic potential. *Phys. Chem. Chem. Phys.* **2002**, *4*, 4353−4359.
(39) Bader, R. F. W. Atoms in Molecules. *Acc. Chem. Res.* **1985**, *18*, 9−15.
(40) Popelier, P. L. A. *Atoms in Molecules. An Introduction*; Pearson Education: London, 2000.
(41) Bader, R. F. W. *Atoms in Molecules. A Quantum Theory*; Oxford Univ. Press: Oxford, Great Britain, 1990.
(42) Rafat, M.; Devereux, M.; Popelier, P. L. A. Rendering of quantum topological atoms and bonds. *J. Mol. Graphics Modell* **2005**, *24*, 111−120.
(43) Bader, R. F. W.; Gatti, C. A Green's function for the density. *Chem. Phys. Lett.* **1998**, *287*, 233−238.
(44) Popelier, P. L. A. Quantum molecular similarity. 1. BCP space. *J. Phys. Chem. A* **1999**, *103*, 2883−2890.
(45) Popelier, P. L. A. Developing Quantum Topological Molecular Similarity (QTMS). In *Quantum Biochemistry: Electronic Structure and Biological Activity*; Matta, C. F., Ed.; Wiley-VCH: Weinheim, Germany, 2010; Vol. *Part IV*; pp 669−692.
(46) Bader, R. F. W.; Essen, H. The Characterization of Atomic Interactions. *J. Chem. Phys.* **1984**, *80*, 1943−1960.
(47) O'Brien, S. E.; Popelier, P. L. A. Quantum molecular similarity. Part 2: The relation between properties in BCP space and bond length. *Can. J. Chem.* **1999**, *77*, 28−36.
(48) O'Brien, S. E.; Popelier, P. L. A. Quantum Molecular Similarity. Part 3: QTMS descriptors. *J. Chem. Inf. Comput. Sci.* **2001**, *41*, 764−775.
(49) Frisch, M. J.; Trucks, G. W.; Schlegel, H. B.; Scuseria, G. E.; Robb, M. A.; Cheeseman, J. R.; Montgomery, J. A., Jr.; Vreven, T.; Kudin, K. N.; Burant, J. C.; Millam, J. M.; Iyengar, S. S.; Tomasi, J.; Barone, V.; Mennucci, B.; Cossi, M.; Scalmani, G.; Rega, N.; Petersson, G. A.; Nakatsuji, H.; Hada, M.; Ehara, M.; Toyota, K.; Fukuda, R.; Hasegawa, J.; Ishida, M.; Nakajima, T.; Honda, Y.; Kitao, O.; Nakai, H.; Klene, M.; Li, X.; Knox, J. E.; Hratchian, H. P.; Cross, J. B.; Bakken, V.; Adamo, C.; Jaramillo, J.; Gomperts, R.; Stratmann, R. E.; Yazyev, O.; Austin, A. J.; Cammi, R.; Pomelli, C.; Ochterski, J. W.; Ayala, P. Y.; Morokuma, K.; Voth, G. A.; Salvador, P.; Dannenberg, J. J.; Zakrzewski, V. G.; Dapprich, S.; Daniels, A. D.; Strain, M. C.; Farkas, O.; Malick, D. K.; Rabuck, A. D.; Raghavachari, K.; Foresman, J. B.; Ortiz, J. V.; Cui, Q.; Baboul, A. G.; Clifford, S.; Cioslowski, J.; Stefanov, B. B.; Liu, G.; Liashenko, A.; Piskorz, P.; Komaromi, I.; Martin, R. L.; Fox, D. J.; Keith, T.; Al-Laham, M. A.; Peng, C. Y.; Nanayakkara, A.; Challacombe, M.; Gill, P. M. W.; Johnson, B.; Chen, W.; Wong, M. W.; Gonzalez, C.; Pople, J. A. *Gaussian 03*, revision C.02; Gaussian, Inc.: Wallingford, CT, 2004.
(50) Popelier, P. L. A. A method to integrate an atom in a molecule without explicit representation of the interatomic surface. *Comput. Phys. Commun.* **1998**, *108*, 180−190.
(51) Griffiths, M. Z.; Popelier, P. L. A.: Characterising heterocyclic rings through Quantum Chemical Topology. In *Topics in Heterocyclic Chemistry*; Geerlings, P., de Proft, F., Eds.; Springer: Germany, 2013; in the press.